Horizontal Velocities in a Global Reference Frame Derived from Sentinel-1 Along-track Interferometry

Milan Lazecky, Andrew J. Hooper

University of Leeds, UK (COMET)

PRESENTED AT:

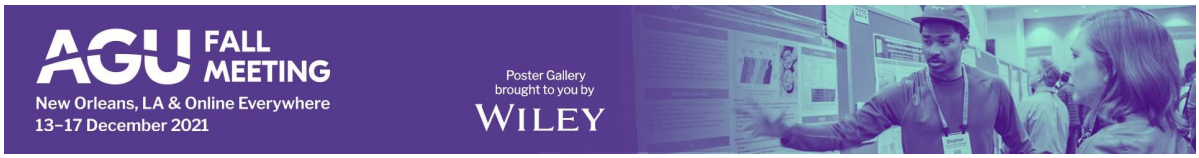

INTRODUCTION

With the Copernicus Sentinel-1 Synthetic Aperture Radar (SAR) satellites, the geoscience community acquired a unique tool for measuring precise motion of tectonic plates. The Centre for Observation and Modelling of Earthquakes, Volcanoes and Tectonics (COMET) LiCSAR system (Lazecky et al., 2020) routinely generates Sentinel-1 differential interferograms over tectonic (and volcanic) areas, and carries out interferometric (InSAR) time series analyses to measure surface deformation in the satellite line-of-sight (LOS) direction.

The InSAR measurements can be then used to derive vertical and horizontal motion components, but the LOS sensitivity is very low for the N-S motion component that must be estimated using available GNSS data (Weiss et al., 2020). A relatively new approach exploiting azimuth (or, along-track) subpixel shifts proved appropriate precision for measuring N-S component of large-scale deformations (Li et al., 2021), allowed by exploiting Sentinel-1 data taken in the Interferometric Wide Swath (IWS) acquisition mode, that is an implementation of Terrain Observation with Progressive Scan (TOPS) mode (Yague-Martinez et al., 2016). Hereby, we investigate the azimuth shifts in relatively large blocks (approx. 250x250 km), in order to observe large-scale tectonic motion and characterise some of the error sources, such as the solid Earth tides and ionosphere.

In total, we have selected 107,476 azimuth shift (daz) values over 1,063 LiCSAR frame units that pass the condition of a minimum count of 30 daz values existing per frame. As the LiCSAR processing currently concentrates on the Asian part of the Alpine-Himalayan Belt (AHBa), we provide outputs of our analyzes in both full global dataset and the AHBa subset, defined by bounding box of 25°-110°/25°-45° in longitude/latitude. These values were investigated to acquire large-scale (tectonic plates) motion estimates that were compared to the ITRF2014 plate motion model (PMM) (Altamimi et al., 2017).

GENERATING MOTION RATES FROM AZIMUTH SHIFTS

Generation of daz values

We extract the Level-1 single look complex (SLC) data of the standard Sentinel-1 IWS burst units, and process and merge those bursts into larger spatial units defined as frames. One standard frame consists of 13 bursts per each of 3 swaths and covers an area of approx. 250x250 km. We perform standard procedure to resample IWS data of each set of acquisitions per orbit cycle (epoch) towards a reference epoch of a frame unit. The azimuth subpixel shift da values of each frame epoch, w.r.t. reference, are estimated during the resampling process.

We apply Copernicus Sentinel-1 Precise Orbit Determination (POD) ephemerides to the input epoch SLC and resample to the geometry of the reference epoch SLC considering heights w.r.t. WGS-84 ellipsoid (where a DEM-simulated SAR amplitude has been fit to the POD-refined reference epoch SLC), using standard approach by GAMMA SAR processing software (command rdc_trans). We then run several iterations of intensity cross correlation (ICC) on the input epoch SLC data to estimate a sub-pixel shift in (both range and) azimuth (da_{ICC}) directions to the precision of around 0.01 pixels, w.r.t. the reference epoch. We then resample the SLC to an intermediate product and iteratively estimate the azimuth coregistration offset da_{SD} based on a spectral diversity (SD) of burst overlaps with either the reference epoch or another previously resampled epoch SLC (RSLC3) if closer in time to the input epoch SLC. This operation aims to refine azimuth shift values to the precision of around 0.0005 pixels but is additionally affected by dispersive effects of especially the electron content in ionosphere (Gomba et al., 2016).

We sum the estimates from both ICC and SD into the final da values, as input to the following analysis. We also extract other relevant information on frame basis, including ground footprint heading angle within the frame scene α (further as heading, or the ground azimuth direction), ground pixel resolution in the azimuth direction r_{azi}, average incidence angle within the whole scene θ_{inc} and Doppler centroid frequency range within a burst df_{DC}. The azimuth pixel shift da would be observed in the SD phase $d\Phi_{SD} = d\Phi(n)-d\Phi(n+1)$, where dΦ is an interferometric phase difference in the overlap between bursts numbers n, n+1 of two evaluated epochs and the azimuth pulse repetition frequency PRF is from azimuth time interval t^{-1}, and thus

$$\Delta a = \Delta a_{ICC} + \Delta a_{SD} = \Delta a_{ICC} + PRF\frac{\Delta\Phi_{SD}}{2\pi\Delta f_{DC}}.$$

The azimuth pixel offset shift da would be related to the shift corresponding to a ground displacement observation. Therefore and for convenience, we further use term daz values [mm], as a ground displacement measured in azimuth, calculated as daz = da * r_{azi}.

Correction of daz shift due to POD change

The POD products of Sentinel-1 satellites changed at the end of July 2020 to the version 1.7, incorporating correction of the on-board GPS Antenna Reference Point (ARP) position (Peter et al., 2020).

This correction implied a 3-D position change of approx. 6 cm and led into a full reprocessing of the Sentinel-1 POD archive, published in 2021 as CPOR products. The correct position of ARP is shifted by 39 mm in the along-track direction of the satellite (Fernandez et al., 2019). We have applied this correction and confirmed significant decrease of RMSE when daz values are estimated from data using the updated POD products (Lazecky and Hooper, 2021, in print).

Estimation of azimuth velocities

We have corrected the daz values for their median per frame, mainly related to daz shift of the reference epoch, corrected daz values due to the POD change shift, and estimated a linear trend to represent horizontal motion velocity v_{azi} of the frame, having outliers removed by the Huber regression method applied with parameters alpha=1.0 and epsilon=1.35.

We have used the final linear fit model to calculate RMSE σ_{daz} from all daz measurements per frame. We have then used σ_{daz} values to calculate RMSE σ_v of v_{azi} by solving the weighted least squares solution error Q_m by

$$Q_m = [A^T Q_d^{-1} A]^{-1};\ Q_d = \sigma_{daz}^2 I_N;\ diag(Q_m) = (\sigma_v^2, \sigma_c^2)$$

where I_N is an NxN identity matrix for N daz values and A represents an Nx2 matrix of acquisition time t [years] and a constant offset (not used further).

DECOMPOSITION TO N, E AND COMPARISON TO ITRF2014 PLATE MOTION MODEL

In order to decompose the daz-based estimates of horizontal displacement velocity $v_{azi,D}$, $v_{azi,A}$ in the satellite azimuth direction from descending (D) and ascending (A) tracks, respectively, to N, E direction components, v_N and v_E, we establish a global grid with a pixel size of 250x250 km, map overlapping frames (having their centroid inside the common grid cell) and calculate $v = [v_E, v_N]$ for cells having both A and D frames in overlap, similar to (Wright et al., 2009). We have estimated precision of measurements in each motion component per grid cell, based on σ_v estimates of respective frames in the fashion of solving weighted least squares solution error allowing to acquire RMSE $\sigma_{v,E}$ and $\sigma_{v,N}$ of v_E, v_N in E, N directions, respectively.

We have then filtered the dataset for outliers and investigated accuracy of the estimates by comparison with the ITRF2014 PMM E, N velocity estimates $v_{PMM} = [v_{E,PMM}, v_{N,PMM}]$, extracted as an average per a set of coordinates within each of the grid cells.

We visualize the constructed decomposition grid and E, N velocities by both PMM and the final daz-based estimates after both solid Earth tides (SET) and ionospheric corrections, $v_{E,nTI}$, $v_{N,nTI}$ in Figure 1 below. At the bottom subplots (difference v_{nTI} - v_{PMM}), the figure allows to identify spatial patterns of a higher deviation from the model, e.g. a higher v_E of the E part of AHBa area or an increased westward motion of Turkey as can be expected (Weiss et al., 2020), w.r.t. PMM. This is further visible in the following Figure 2 that provides a visual comparison of motion vectors from the PMM and decomposed daz-based measurements based on both $v_{azi,nTI}$ and $v_{azi,nT}$, over the AHBa region.

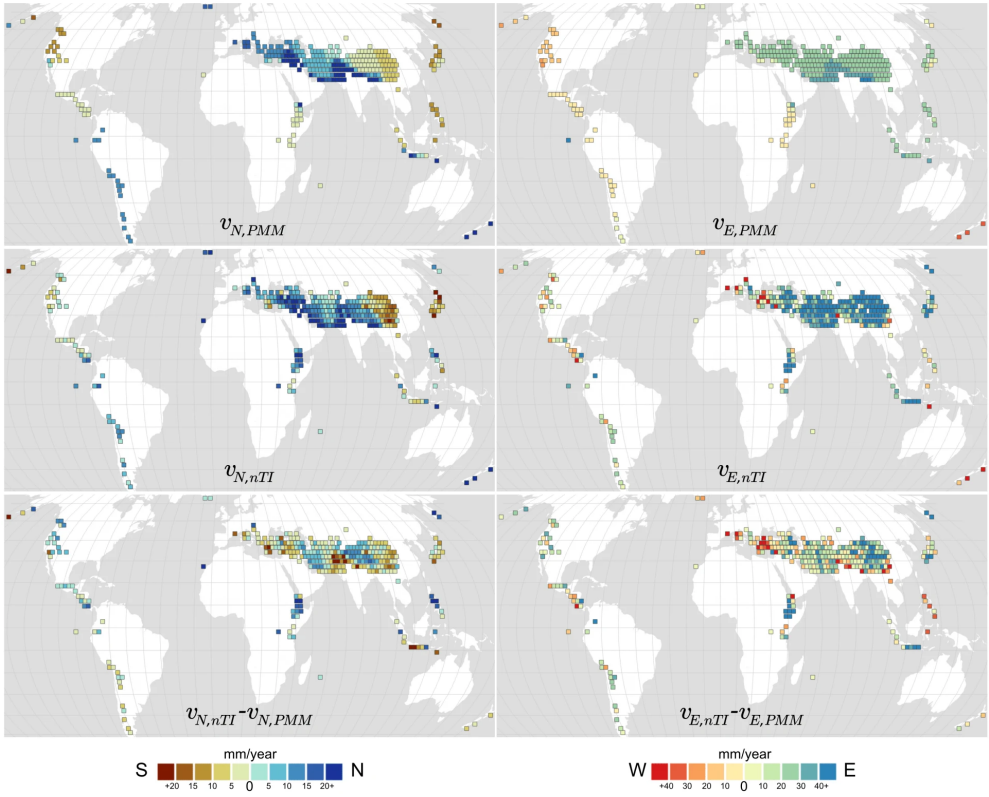

Fig. 2 below shows generally better fit of v_{nTI} values over v_{nT} to the PMM in terms of direction of the motion but with often higher estimated velocity. This was enumerated in Tab. 1 as the median difference between vector direction γ_{nT}, γ_{nTI} (and length A_{nT}, A_{nTI}) and corresponding values from the PMM in both AHBa region and the global dataset.

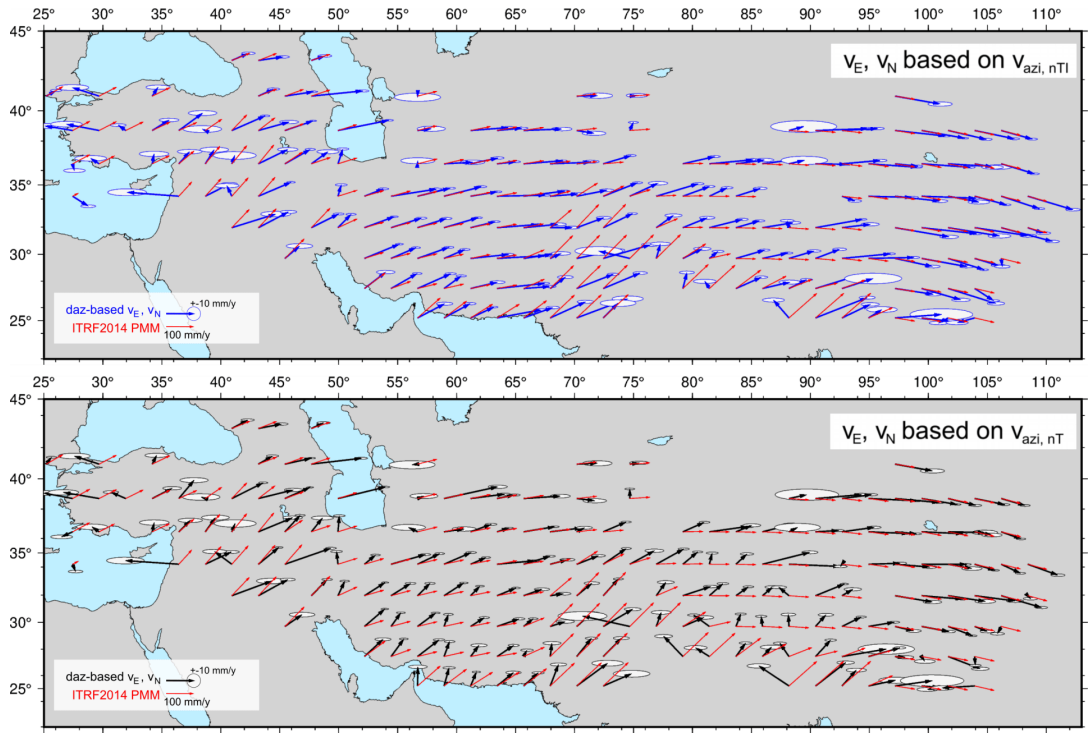

For a statistic evaluation of the quality of our estimates, we have used median values of v and σ_v at both full dataset (253 grid cells) and the AHBa subset (188 grid cells) in Table 1 that also includes similar comparison of the original estimates in the azimuth direction.

It is visible from the table that the ionospheric correction (affecting mainly ascending frames) induced an overall increase of velocity estimates in the E component v_E, and in case of AHBa subset, it increased also $\sigma_{v,E}$. Yet, the main component of interest, v_N, appears closer to the values expected by the PMM.

Table 1. Median values of estimated velocities v [mm/year] and their RMSE (σ) [mm/year] demonstrating impact of SET (nT) plus ionospheric (nTI) corrections on v_{azi} and decomposed v_E,v_N, and median deviations of vector angle γ and length A of v_E,v_N from the ITRF2014 PMM values, in both global dataset and the AHBa subset.

global dataset

track	$\overline{v_{azi,PMM}}$	$\overline{v_{azi}} \pm \overline{\sigma_v}$	$\overline{v_{azi,nT}} \pm \overline{\sigma_{v,nT}}$	$\overline{v_{azi,nTI}} \pm \overline{\sigma_{v,nTI}}$
ascending	0.0	3.2 ± 4.1	3.2 ± 4.0	1.4 ± 3.9
descending	-7.5	-10.4 ± 3.6	-10.1 ± 3.5	-10.2 ± 3.5
direction	$\overline{v_{PMM}}$	$\overline{v} \pm \overline{\sigma_v}$	$\overline{v_{nT}} \pm \overline{\sigma_{v,nT}}$	$\overline{v_{nTI}} \pm \overline{\sigma_{v,nTI}}$
E-W	28.2	20.1 ± 13.5	22.1 ± 11.3	36.4 ± 11.4
N-S	5.7	9.9 ± 2.6	9.2 ± 2.2	7.4 ± 2.1

AHBa subset

track	$\overline{v_{azi,PMM}}$	$\overline{v_{azi}} \pm \overline{\sigma_v}$	$\overline{v_{azi,nT}} \pm \overline{\sigma_{v,nT}}$	$\overline{v_{azi,nTI}} \pm \overline{\sigma_{v,nTI}}$
ascending	0.7	7.4 ± 2.8	6.7 ± 2.7	2.3 ± 2.7
descending	-11.0	-15.8 ± 2.5	-15.6 ± 2.4	-15.2 ± 2.4
direction	$\overline{v_{PMM}}$	$\overline{v} \pm \overline{\sigma_v}$	$\overline{v_{nT}} \pm \overline{\sigma_{v,nT}}$	$\overline{v_{nTI}} \pm \overline{\sigma_{v,nTI}}$
E-W	28.5	20.6 ± 12.1	25.9 ± 10.2	41.0 ± 10.0
N-S	6.3	11.9 ± 2.2	12.1 ± 1.8	8.5 ± 1.8

median deviations from the ITRF2014 PMM

dataset	$\overline{\Delta\gamma_{nT,PMM}}$	$\overline{\Delta\gamma_{nTI,PMM}}$	$\overline{\Delta A_{nT,PMM}}$	$\overline{\Delta A_{nTI,PMM}}$
global	6.7 deg	0.9 deg	1.8 mm/year	11.5 mm/year
AHBa	8.5 deg	1.2 deg	-1.2 mm/year	11.5 mm/year

ESTIMATION AND EFFECTS OF DAZ INFLUENCE FACTORS

We have performed correction of daz on solid Earth tides (SET), marked as 'nT' for 'no tides' (daz_{nT}) and ionosphere I, leading to daz_{nTI} (nTI for no-tides-no-ionosphere), prior to estimation of the horizontal velocity estimates $v_{azi,nT}$ and $v_{azi,nTI}$, respectively.

Figure 3 demonstrates the influence of the implemented corrections applied on the original daz values. The time series are based on median-corrected daz values, filtered by a rolling median using 10 samples, and plotted by a colour gradient representing distance of each frame centre from the Earth equator.

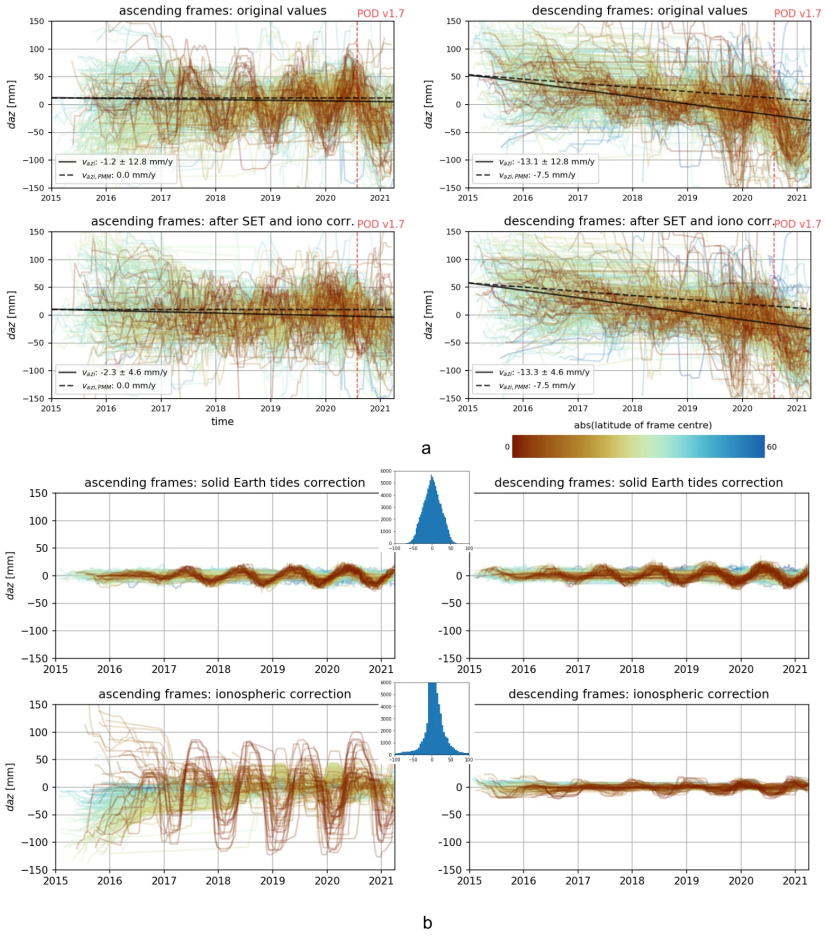

For SET, we used model 'solid' implemented to GMT software. For ionosphere, we used the IRI2016 model based on data available at relatively low frequency (months). We expect this model to be sufficient for reduction of seasonal fluctuations of daz caused by ionospheric influence but not for a precise estimate per each daz sample.

We have investigated the correction effect on RMSE w.r.t. the velocity estimates, as well as deviation from the expected rates by ITR2014 plate motion model (PMM) projected to the azimuth direction ($v_{azi,PMM}$). As shown in Fig. 3, the v_{azi} values deviate from $v_{azi,PMM}$ by medians of -2.3 mm/year for A and -5.8 mm/year for D frames. The deviation slightly increased after the applied corrections (note that for this preliminary assessment, we have used only daz values prior to the date of a significant change of POD products to version 1.7).

The effects of SET and ionospheric corrections, e.g. a decrease of the RMSE of v_{azi} values, are documented in Table 1 based on the final dataset (including the daz correction related to the POD change).

Conversion of model parameters to azimuth direction

We consider several sources of daz, or da, and calculate an average value per frame in given temporal epoch w.r.t. frame reference epoch using dedicated models. We project E, N components of each modeled shift dE_x, dN_x to the satellite azimuth direction pixel offset da_x by

$$\Delta a_x = \frac{dE_x \ \sin(\alpha) + dN_x \cos(\alpha)}{r_{azi}}.$$

using heading angle α and azimuth pixel resolution r_{azi}, per frame.

For SET term, the operation is straightforward from estimated dE, dN shifts.

For ionosphere, we have performed the ionospheric phase advance modelling as an inverted approach to (Gomba et al., 2016) for evaluation of ionospheric influence on SD values. We use IRI2016 model to estimate total electron content (TEC) between the satellite and the scene valid for the central burst overlap, i.e. vertical TEC column (TECv), for points A, B inbetween the satellite nadir position during acquiring the point in the centre of the overlap between a forward-looking (A) and backward-looking (B) burst, respectively, at the centre of the frame scene.

We calculate the location of points A, B per each epoch, following the azimuth direction footprint below the ionosphere piercing point (IPP) located in the LOS at the height of the ionospheric F2 layer peak (H_{iono}), also estimated by IRI2016 per each temporal epoch.

We estimate incidence angle θ_{IPP} and use it to convert modeled TECv column to the line-of-sight/slant direction (TECs), as:

$$TEC_s = \frac{TEC_v}{\sqrt{1 - \sin \Theta_{IPP}{}^2}} = \frac{TEC_v}{\sqrt{1 - (\frac{R \sin \Theta}{R + H_{iono}})^2}}$$

where R is the Earth radius.

The TECs difference should approximately correspond to the ionospheric influence of the SAR carrier wave of frequency f_0, modulated by the satellite motion and antenna steering during the TOPS acquisition mode in the frequency range of f_H, $f_L = f_0 \mp 0.5\ df_{DC}$ at the burst edges.

We have derived da_{iono} towards the frame reference epoch as

$$\Delta a_{iono} = 2PRF\,K \frac{f_0}{c\,\Delta f_{DC}} \left(\frac{\Delta TEC_s(B)}{f_L^2} - \frac{\Delta TEC_s(A)}{f_H^2} \right)$$

where PRF=486.486 Hz is a pulse repetition frequency (azimuth sampling rate), K = 40.308193 m^3/s^2 is a commonly applied valid constant (Hoque and Jakowski, 2021), c is the generic constant of the speed of light in vacuum, and dTECs is a difference between TECs estimate in each temporal epoch and the reference epoch, at coordinates of the given point.

Note that $df_{DC}=f_H - f_L = -(f(B)-f(A))$ and the ionospheric effect accounted for is a (negative sign) phase advance, together leading to the plus sign of the equation. Also note that no effect induced by the absolute magnitude of dTEC on the azimuth shift is expected (Fattahi et al., 2017).

DISCUSSION AND CONCLUSIONS

We have investigated possibility of precise measurements of large-scale horizontal motion using azimuth shifts estimated from Sentinel-1 IWS data, in this case using average values in 250x250 km cells, globally, processed within COMET LiCSAR system. The precision significantly improves after incorporating correction for solid Earth tides and, especially in latitudes closer to the equator, ionospheric influence. However, our corrections probably removed only a part of the non-deformation component of daz values, partially due to imperfections of applied models.

The daz estimations can be considered along-track measurements that are attached to the global ECEF NNR framework by GPS-based positioning of Sentinel-1 satellites. Our daz-based velocity estimates and their consequent N, E motion vector estimates fit reasonably well with the ITRF2014 PMM, although discrepancies exist and were documented in this work. Our final corrected dataset shows a higher overall shift towards E in the AHBa region, on the other hand our estimates correctly identified a westward motion of Anatolia that was probably not incorporated to the ITRF2014 PMM.

We have investigated and incorporated correction due to new POD v1.7 specifications that shift daz values after 2020-07-30 by daz_{ARP}=-39 mm that allowed for a seamless combination of all available daz values for precise velocity estimates. We have observed an increased precision of daz processed using the updated POD v1.7.

Further works

Further research should also include across-track (range pixel offset, or LOS InSAR time series) measurements in combination to the along-track InSAR approach and other available measurements, in order to improve the ITRF2014 PMM and support knowledge on Earth plate motion dynamics.
We prepare a solution to share the original daz values within the community, as an additional new open product of the COMET LiCSAR system. Also both data and codes for this work will be available as part of (Lazecky and Hooper, 2021).

The list of factors influencing daz is not comprehensive. For example we did not estimate daz due to N-S gradients of large scale tropospheric bodies as monsoons, although it technically is possible to model using e.g. GACOS services/ECMWF model. Also, we did not incorporate ocean tidal loading and we intend to study the effects of the improved ETERNA model (Ducarme and Schuller, 2018). The estimates available within S1_ETAD products (Gisinger et al., 2021) should be compared and incorporated in a future study.

We are aware of low spatial and temporal resolution of the applied IRI2016 model for ionospheric corrections. We have observed large variations of daz values at the end of solar cycle 24 peak that are probably not fully corrected, and we expect similar effects in the period behind the investigated dataset. We did not apply another model of ionosphere.

Finally, we have observed a residual periodic annual signal, especially in frames closer to the equator, for both descending (dawn) and ascending (dusk) frames, perhaps due to another solar-related cause, subject to further studies (assuming atmospheric variables affecting propagation of the electromagnetic signal).

On comparison to ITRF2014 PMM

Our observations show an overall along-track motion trend for descending frames, of a higher velocity than expected by ITRF2014 PMM. While N-S motion estimates offer relatively good fit to the values expected by ITRF2014 PMM, the E-W component is also largely deviating, especially after ionospheric correction that caused an increase of estimated E velocity component over most of AHBa area. As far as we understand, the daz measurements are w.r.t. satellite positions that are located in the Earth-centered Earth-fixed (ECEF) frame in a no-net-rotation (NNR) framework, same as the ITRF2014 PMM values used here. The global net rotation of litospheric plates is expected around 15 mm/year westwards (Torsvik et al., 2010), not observed by our measurements.

The coregistration procedure aims to provide daz estimates in the precision of up to 7 mm (0.0005 pixels). Due to the cascade strategy in coregistration, the coregistration errors may propagate in time. However our analysis did not identify significant error propagation (Lazecky and Hooper, 2021).

Acknowledgments

This work is supported by The Natural Environment Research Council large grant, “Looking inside the continents from Space” (NE/K010867/1). COMET is the NERC Centre for the Observation and Modelling of Earthquakes, Volcanoes and Tectonics, a partnership between UK Universities and the British Geological Survey.

The authors want to thank other experts that helped finalising this work by sharing their knowledge in discussions, we thank namely Dr. Heike Peter, Dr. Pawan Piromthong, Dr. Chris Rollins and Dr. Jonathan Weiss.

REFERENCES

Altamimi, Z., Metivier, L., Rebischung, P., Rouby, H., & Collilieux, X. (2017). ITRF2014 plate motion model.Geophysical Journal International,209(3), 1906-1912. doi: 10.1093/gji/ggx136

Bilitza, D., Altadill, D., Truhlik, V., Shubin, V., Galkin, I., Reinisch, B., & Huang, X.(2017). International reference ionosphere 2016: From ionospheric climate to real-time weather predictions. Space Weather,15(2), 418-429. doi: 10.1002/2016SW001593

Ducarme, B., & Schuller, K. (2018). Canonical wave grouping as the key to optimal tidal analysis.Bulletin d'Informations Marees Terrestres (BIM),150, 12131–12244.

Fattahi, H., Simons, M., & Agram, P. (2017). Insar time-series estimation of the ionospheric phase delay: An extension of the split range-spectrum technique.IEEE Transactions on Geoscience and Remote Sensing,55(10), 5984-5996. doi: 10.1109/TGRS.2017.2718566

Fernandez, M., Aguilar, J. A., & Fernandez, J. (2019).Sentinel-1 properties for gps pod: Copernicus sentinel-1, -2, and -3 precise orbit determination service (sentinelspod). https://sentinels.copernicus.eu/documents/247904/3455957/Sentinel-1-properties-for-GPS-POD (https://sentinels.copernicus.eu/documents/247904/3455957/Sentinel-1-properties-for-GPS-POD)

Gisinger, C., Schubert, A., Breit, H., Garthwaite, M., Balss, U., Willberg, M., . . . Miranda, N. (2021). In-depth verification of sentinel-1 and terrasar-x geolocation accuracy using the australian corner reflector array. IEEE Transactions on Geoscience and Remote Sensing,59(2), 1154-1181. doi: 10.1109/TGRS.2019.2961248

Gomba, G., Parizzi, A., De Zan, F., Eineder, M., & Bamler, R. (2016). Toward operational compensation of ionospheric effects in sar interferograms: The split-spectrum method. IEEE Transactions on Geoscience and Remote Sensing,54(3), 1446-1461. doi: 10.1109/TGRS.2015.2481079

Hoque, M., & Jakowski, N. (2012). Ionospheric propagation effects on gnss signals and new correction approaches. doi: 10.5772/30090

Lazecky, M., Spaans, K., Gonzalez, P. J., Maghsoudi, Y., Morishita, Y., Albino, F., . . ., Wright, T. J. (2020). Licsar: An automatic insar tool for measuring and monitoring tectonic and volcanic activity. Remote Sensing,12(15). doi: 10.3390/rs12152430

Lazecky, M., Hooper, A., 2021. Horizontal velocities in a global reference frame from Sentinel-1 along-track sub-pixel offsets. Sent to GRL 2021 for review. Pre-print:

Li, X., Jonsson, S., & Cao, Y. (2021). Interseismic deformation from sentinel-1 burst-overlap interferometry: Application to the southern dead sea fault. Earth and Space Science Open Archive, 13. doi: 10.1002/essoar.10506585.1

Peter, H., Fernandez, J., & Femenias, P. (2020). Copernicus sentinel-1 satellites: sensitivity of antenna offset estimation to orbit and observation modelling. Advances in Geosciences, 50, 87–100. doi: 10.5194/adgeo-50-87-2020 (https://adgeo.copernicus.org/articles/50/87/2020/)

Torsvik, T. H., Steinberger, B., Gurnis, M., & Gaina, C. (2010). Plate tectonics and net lithosphere rotation over the past 150my. Earth and Planetary Science Letters,291(1),106-112. doi: 10.1016/j.epsl.2009.12.055

Weiss J. R., Walters, R. J., Morishita, Y., Wright, T. J., Lazecky, M., Wang, H., Parsons, B. et al. (2020). High-resolution surface velocities and strain for anatolia from sentinel-1 insar and gnss data. Geophysical Research Letters,47(17), doi: 10.1029/2020GL087376 (https://doi.org/10.1029/2020GL087376)

Wright TJ, Parsons BE, Lu Z. 2004. Toward mapping surface deformation in three dimensions using InSAR. GEOPHYS RES LETT. 31(1), doi: 10.1029/2003GL018827 (https://agupubs.onlinelibrary.wiley.com/doi/full/10.1029/2003GL018827)

Yague-Martınez, N., Prats-Iraola, P., Rodrıguez Gonzalez, F., Brcic, R., Shau, R., Geudtner, D., . . . Bamler, R. (2016). Interferometric processing of sentinel-1 tops data.IEEE Transactions on Geoscience and Remote Sensing, 54(4), 2220-2234. doi: 10.1109/TGRS.2015.2497902